Spectrochimica Acta Part A: Molecular and Biomolecular Spectroscopy 234 (2020) 118229

Contents lists available at ScienceDirect

Spectrochimica Acta Part A: Molecular and Biomolecular Spectroscopy

journal homepage: www.elsevier.com/locate/saa

Detecting melanoma with a terahertz spectroscopy imaging technique

Dandan Li [a,b,1], Zhongbo Yang [b,1], Ailing Fu [c], Tunan Chen [d], Ligang Chen [b,c], Mingjie Tang [b], Hua Zhang [b], Ning Mu [d], Shi Wang [d], Guizhao Liang [a,*], Huabin Wang [b,*]

[a] Key Laboratory of Biorheological Science and Technology, Ministry of Education, Chongqing University, Chongqing 400044, China
[b] Chongqing Engineering Research Center of High-Resolution and Three-Dimensional Dynamic Imaging Technology & Research Center of Applied Physics, Chongqing Institute of Green and Intelligent Technology, Chinese Academy of Sciences, Chongqing 400714, China
[c] School of Pharmaceutical Sciences, Southwest University, Chongqing 400715, China
[d] Department of Neurosurgery, Southwest Hospital, Army Medical University, Chongqing 400038, China

ARTICLE INFO

Article history:
Received 17 December 2019
Received in revised form 22 February 2020
Accepted 3 March 2020
Available online 05 March 2020

Keywords:
Histology
Melanoma
Optical visual imaging
Terahertz imaging
Tissue diseases

ABSTRACT

Transmission mode terahertz time-domain spectroscopy system was employed to image BALB/c mouse skin tissue slices containing melanoma. The melanoma was unambiguously identified in the frequency region of 0.6–1.8 THz because melanoma has a higher refractive index as well as a higher absorption coefficient than the normal region of the skin tissue. Based on the results of hematoxylin-eosin staining and mass weighing, it was further suggested that the higher density of nucleic acids, higher water content, and lower fat content in the melanoma compared to the normal region are major factors responsible for melanoma's higher refractive index and absorption coefficient than normal tissue. The present work validates that terahertz time-domain spectroscopy imaging technique is possible to be used for the diagnosis of melanoma.

1. Introduction

Melanoma is essentially a malignant tumor caused by abnormal proliferation of melanocytes in organism tissues [1,2]. The diagnosis and treatment of melanoma have been attracting intensive public attention worldwide because it accounts for about two-thirds of the total death from skin cancers [3,4]. Since there are no effective treatments available for patients with advanced melanoma, the diagnosis of melanoma at its early stage is key to improve the relative survival rate of the patients [5].

In the past several decades, various methods have been developed and applied for the detection of melanoma, mainly including dermoscopy-based techniques, biopsy and pathology review as well as gene expression [5]. However, the detection of melanoma early in its evolution is still a challenge due to the limitations of these traditional methods. Briefly, for the dermoscopy-based techniques such as the 4-point ABCD rule (asymmetry, border irregularity, color variegation, and diameter > 6 mm) and the 7-point checklist (size change, irregular pigmentation, irregular border, inflammation, itch or altered sensation, diameter > 7 mm, and oozing/crusting), the diagnosis is only based on morphology, so the accuracy is not good [5,6]. For the techniques involving biopsy, pathology and/or gene expression, the methods are invasive, time consuming and health care costly. Therefore, advanced techniques capable of detecting melanoma in its early form are desperately needed, and these approaches should ideally have as many as of the features such as being accurate, sensitive, objective, quantitative, noninvasive, noncontact, low-costs, and easy operation [7].

With the rapid development of high-power and/or high-speed laser sources, high resolution detectors and algorithms for data analysis, over the past two decades, infrared (IR) spectroscopy, Raman spectroscopy and terahertz (THz) spectroscopy based techniques have shown promise for the detection of melanoma [7]. These methods can well meet the requirements for an ideal approach of detecting melanoma. Nevertheless, although THz-based technique has great potential to be applied in clinical diagnosis of melanoma, it is the least explored and developed technique among above-mentioned three techniques because it is much younger than IR spectroscopy and Raman spectroscopy.

THz (1 THz = 10^{12} Hz) radiation [8–11] is an electromagnetic wave whose frequency lies between the IR and microwave regions, namely 0.1 to 10 THz. Its wavelengths and photon energies are ranging from 3 mm to 30 μm, and 0.41 meV to 41 meV, respectively. Owing to its high sensitivity to biomolecules and water contained in biological samples and low ionization of biological samples, THz-based techniques are

* Corresponding authors.
E-mail addresses: gzliang@cqu.edu.cn (G. Liang), wanghuabin@cigit.ac.cn (H. Wang).
[1] These authors contributed equally to this work.

https://doi.org/10.1016/j.saa.2020.118229
1386-1425/

believed to hold great potential in biomedical research and diagnosis [12–15]. Consequently, great efforts have been devoted in the development and application of THz-based techniques in biomedical and biological fields [16–18]. Based on THz spectroscopy and/or spectroscopy imaging techniques, pioneering studies have shown that breast [19], lung [20], pancreas [20] and brain gliomas [21–23] can be identified, which motivated biophysicists to detect melanoma with THz-based techniques. In 2015, Zaytsev et al. [24] detected melanoma precursors from human healthy skin tissues based on the analysis of THz dielectric permittivity curves. In 2017, Park et al. [25] distinguished frozen lymph nodes with melanoma from normal tissues using a THz time-domain spectroscopy (THz-TDS) integration technique. This research greatly enhanced our understanding of melanoma as well as our ability to detect melanoma with THz-based techniques. Nevertheless, so far the underlying mechanisms of discriminating melanoma from normal tissues are still unclear, and relatively little attention has been received from the scientific community to discern melanoma from normal tissues by direct THz spectral imaging despite its significance.

In the present work, we carried out experiments to detect mouse skin tissue containing melanoma at ambient conditions using a THz-TDS imaging technique, combined with the hematoxylin-eosin (HE) staining technique and a mass weighing method for the assessment of water content in the melanoma and the normal tissue. The results show that the melanoma region can be clearly demarcated from the normal region in a wide range of frequency (0.6–1.8 THz). The underlying mechanism is that melanoma has a higher density of nucleic acids, higher water content and lower fat than the normal region, which is responsible for the higher refractive index and absorption coefficient for the melanoma than the normal tissue. The present work confirms that detecting melanoma with the THz-TDS imaging technique is possible.

2. Materials and Methods

2.1. Establishment of Mouse Melanoma Model

Murine B16 melanoma cells (Shanghai Tongwei Biological Technology Co., Ltd., Shanghai, China) were grown in 25 cm^2 tissue culture flasks (Corning Inc., New York, USA) in Roswell Park Memorial Institute Medium (RPMI-1640, Gibco, New York, USA) supplemented with 10% (v/v) fetal bovine serum (FBS, Gibco, New York, USA) and 1% (v/v) penicillin-streptomycin in a 5% CO_2 humidified atmosphere at 37 °C. Cells of logarithmic growth phase were washed with 2 mL of phosphate buffered saline (PBS), digested by 2 mL 0.25% trypsin-EDTA for 2 min, and neutralized with 4 mL of the above cell culture media. After the removal of cell culture media, the cells were mixed gently with a pipette for several times and transferred to a 15 mL tube (Corning Inc., New York, USA) that was centrifuged at 1000 rpm for 5 min. The pellet was re-suspended in 1 mL of PBS for following implanting experiments.

The melanoma model was established by implanting B16 melanoma cells into 10 six-week-old BALB/c mice (Chongqing Medical University, Chongqing, China) with a weight of 20 ± 2 g for each. 200 μL of cell solution (5×10^5 cells/mL) was injected under the skin of the right armpit of each mouse and the mice were allowed to grow for another two weeks for the formation of melanoma. The mice were sacrificed by cervical dislocation and hair removal cream (Laver, Shanghai Weitai Cosmetics Co., Ltd., Shanghai, China) was applied to remove the hair covering the region of the tumor which can be seen as a black nodule. A pair of surgical scissors was used to cut the skin and remove the tissue containing melanoma. For melanoma containing tissues, five were immediately fixed in 4% paraformaldehyde (PFA, Beijing Solarbio Science & Technology Co., Ltd., Beijing, China) at 4 °C for a minimum of 12 h to prevent the possible autolysis [26] prior to the THz test, and other five tissues were embedded by paraffin for HE staining [17,27]. Before performing the animal experiments, approval was granted by the Institutional Animal Care and Use Committee, Chongqing Institute of Green and Intelligent Technology, Chinese Academy of Sciences.

2.2. Tissue Sample Preparation

To prepare tissue samples for THz measurement, PFA-fixed tissue was transferred to a freezing microtome (CM3050S, Leica Biosystems Nussloch GmbH, Nussloch, Germany) and embedded in optimum cutting temperature compound (REF4583, Sakura Finetek USA Inc., Torrance, USA) on the cryostat of the cryomicrotome at −20 °C for 30 min before sectioned into flat slices with an optimized thicknesses of 100 μm [28]. As shown in Fig. 1(b), to prevent tissue dehydration during THz test, each prepared tissue slice was first put in the hole of a double-sided tape, then sandwiched between two polystyrene substrates (PSS) to form a closed environment. The diameter of the hole, thickness of the tape, and thickness of the PSS are 15 mm, 100 μm, and 200 μm, respectively. PSS is almost transparent to broad spectral THz wave, thus it is very suitable to be used as sample support substrates in THz experiments.

2.3. HE Stain

The HE staining technique [29,30] was used to assess the histology of melanoma and normal region of the mouse skin tissue. Briefly, PFA-fixed tissue was embedded in paraffin and sectioned into slices of 3 μm with a rotary microtome (CUT4062, SLEE Medical GmbH, Mainz, Germany). The slices were then de-paraffinized in a xylene bath for 3 min and dried naturally at room temperature. Afterwards, the slices were stained with hematoxylin (C0105, Shanghai Beyotime Biotechnology Co., Ltd., Shanghai, China), followed by counterstaining with eosin (C0105, Shanghai Beyotime Biotechnology Co., Ltd., Shanghai, China). Next, the slices were dehydrated and cleared in sequence by anhydrous ethanol, n-butanol, and xylene for 10 min, respectively. Finally, the slices were mounted with neutral balsam mounting medium (Shanghai Absin Biological Technology Co., Ltd., Shanghai, China), and examined by a microscope slide scanner (Pannoramic MIDI, 3DHISTECH, Ltd., Budapest, Hungary). Ethanol, n-butanol, and xylene are all in analytical grade.

2.4. Set-up for THz-TDS

Tissue slices containing melanoma were characterized by a commercial transmission mode THz-TDS system (Tera K15, Menlo Systems GmbH, Munich, Germany) located in a clean room maintained at a temperature of 22 ± 0.1 °C and a relative humidity of 50 ± 2%. The well controlled experimental condition ensures the high reproducibility of the measurements. The THz-TDS system is illustrated in Fig. 1(a). Briefly, a femtosecond laser was split into the pump beam and the probe beam. The pump beam was irradiated on a biased photoconductive (PC) antenna to emit THz pulse that was pre-collimated by a high-resistivity silicon lens attached behind the PC antenna. Then the pulse was collimated by a polymethylpentene (TPX) lens with an effective focal length of about 50 mm, and focused by another TPX lens. THz pulse transmitted through the sample was detected via a process nearly reverse to the process of THz emission. The optical delay line in the probe optical path was utilized to sample the THz pulse with a time interval and the sampled data were used to rebuild the THz time-domain pulse signal. In THz experiments, the sample was aligned to the focal plane of the incident THz beam and imaged by raster scan with a step size of 0.1 mm for both X and Y axes, and an integration time of 0.5 s for each pixel, under the help of a two-dimensional electric translation stage (M-403.6PD, Physik Instrumente (PI) GmbH & Co. KG, Karlsruhe, Germany). Edge effects at the tissue sample-air border, caused by destructive diffractions in THz imaging, were corrected according to the edge diffraction theory [31], with a self-developed Matlab code (Version R2010a, MathWorks Inc., Natick, USA).

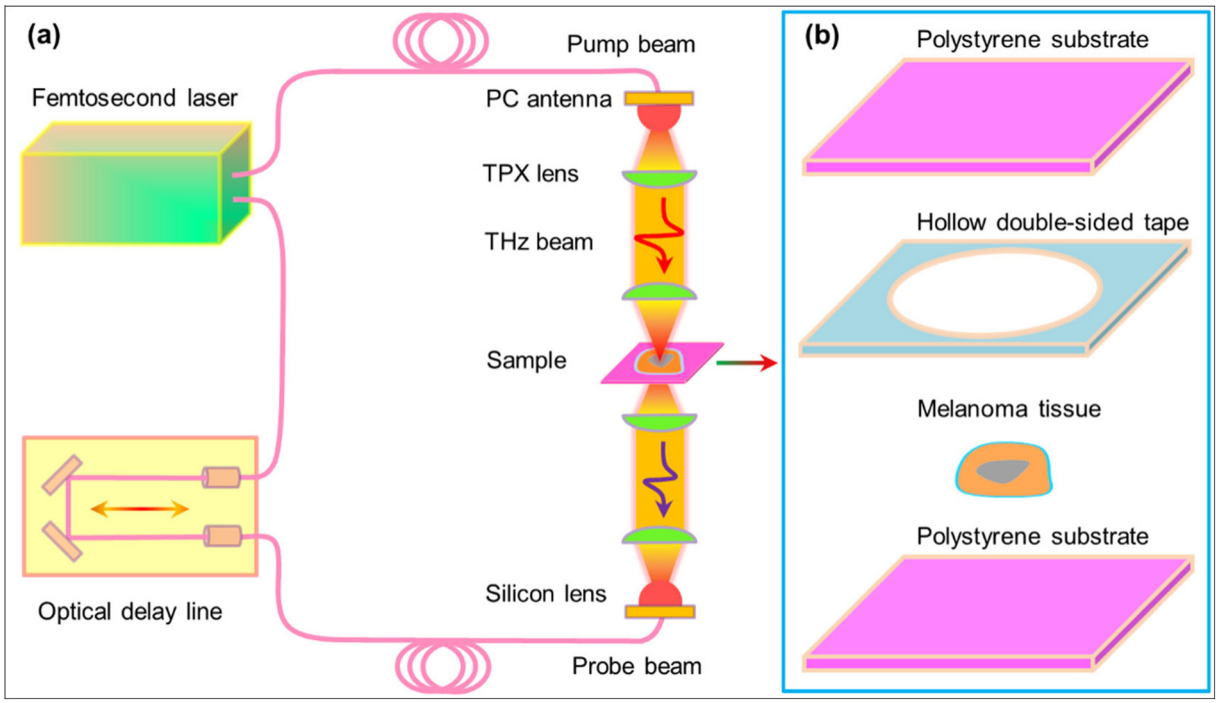

Fig. 1. (a) Schematic of the transmission mode THz-TDS system. (b) Illustration of the components that form an environment-closed sample for THz measurement. The size of the tissue sample is about 6 mm × 6 mm.

2.5. Tissue Water Content by the Weighing Method

A traditional mass weighing method [32] was employed to quantify the water content in fresh pure melanoma tissue and fresh normal tissue surrounding the melanoma, respectively. First, the mass of the tin foil (m_{tf}) was weighed by an electronic balance (ME204E, Mettler Toledo LLC, Columbus, USA) with an accuracy of 0.0001 g. Then, freshly excised mouse tissue (melanoma tissue or normal tissue surrounding the melanoma judged according to the color of the skin) was wrapped in the tin foil, and the gross mass of the foil-wrapped tissue sample (m_{gf}) was weighed immediately. After that, the sample was placed in an oven (BGZ-76, Shanghai Boxun Industry & Commerce Co., Ltd., Shanghai, China) and heated at 100 °C for 30 h to remove the water from the sample. Next, the sample was taken out of the oven and cooled down to room temperature, naturally, and weighed again to obtain the gross mass of the dry sample (m_{gd}). The net mass of fresh tissue (m_{nf}), dry tissue (m_{nd}), and the water content (η) can be calculated via the following equations:

$$m_{nf} = m_{gf} - m_{tf} \tag{1}$$

$$m_{nd} = m_{gd} - m_{tf} \tag{2}$$

$$\eta = \frac{m_{nf} - m_{nd}}{m_{nf}} \times 100\% \tag{3}$$

2.6. Statistical Analysis

The cell numbers in the melanoma region and the adipose region have been counted from HE staining images to compare the cell densities. The statistical data were collected on five different mouse skin tissues containing melanoma. For each sample, the cells were counted from randomly picked six different areas (100 μm × 50 μm) in the adipose region and the melanoma region, respectively. As a result, the cells in 30 different areas for each type of region have been counted. To assess the water content in the melanoma and the normal tissue, 30 melanoma samples and 30 normal skin tissue samples were measured. These samples were freshly excised from 30 mice bearing melanoma and directly used for the experiment. Origin 8.5 software (OriginLab Co., Northampton, USA) was used for the statistical analysis of the data and $P < .01$ was considered statistically significant. The data are presented in mean ± standard deviation. The significance of the data was analyzed by pair sample *t*-test analysis of hypothesis testing.

3. Result and Discussion

3.1. Comparison Optical Visual Image and HE Staining Image of Mouse Skin Tissue Containing Melanoma

In our experiments, we used both optical visual imaging and HE staining techniques to determine melanoma and the normal region of a mouse skin tissue (Fig. 2). By comparing the results, it was found that melanoma could be identified based on visually observed much darker color than the normal region when the thickness of the sample is ≥100 μm because the darker region matches well with the identified melanoma by HE stain.

3.2. THz Image of Mouse Skin Tissue Containing Melanoma

In order to obtain THz image of the skin tissue at different frequencies, the measured THz time-domain electric field ($E(t)$) was transformed into frequency-domain electric field ($E(f)$) by the fast Fourier transform (FFT) algorithm [11], from which THz images can be constructed by THz intensity data ($I = E(f)^2$) at a various of specific frequencies. A typical example was shown in Fig. 3, in which THz images at three different frequencies (1.09, 1.3, and 1.5 THz) are presented. Since the melanoma and the normal region in the tissue slices can be determined from the optical visual image (Fig. 2), the optical visual image of the tissue sample can be used to verify the performance of THz imaging. By comparing the optical visual image and THz images, it was found that both the melanoma region (marked out by green dashed contour lines) and the majority of normal region in the skin tissue were clearly identified. From the image, it can also be concluded that less THz

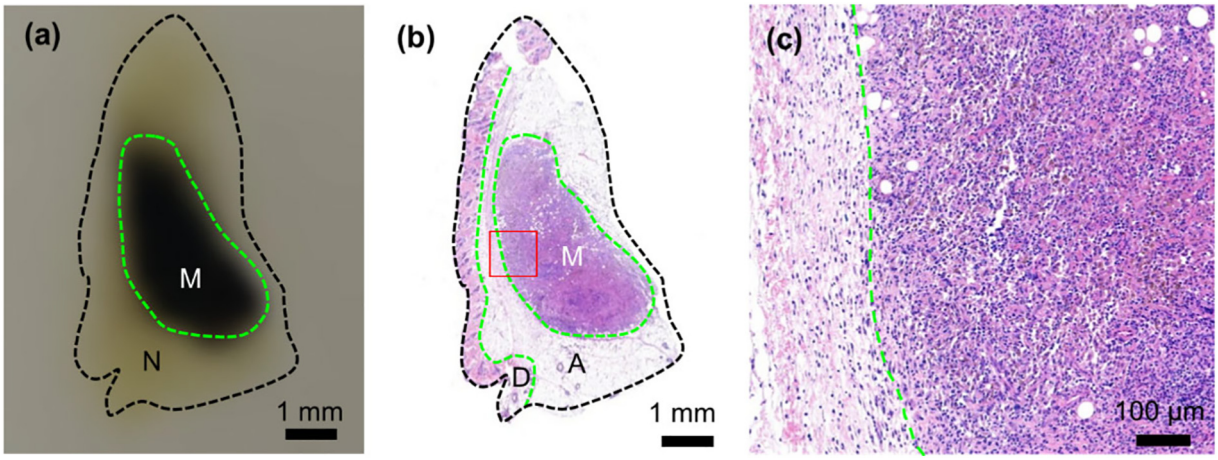

Fig. 2. Identification of melanoma from the mouse skin tissue. (a) Optical visual image of the tissue in which 'M' indicates melanoma outlined by dashed green line, and 'N' indicates normal tissue outlined by dashed black line. (b) HE stained image of the tissue in which 'M' indicates 'melanoma', 'A' indicates adipose region, and 'D' indicates the region formed by dermis and epidermis. The adipose region (A) and the dermis and epidermis region (D) form the normal region (N). The melanoma and the normal region in (a) and (b) are consistent to each other, correspondingly (c) HE stained image corresponding to the region indicated by the red square in (b). From (c), the boundary of the adipose region and the melanoma region can be clearly demarcated. (For interpretation of the references to color in this figure legend, the reader is referred to the web version of this article.)

transmitted through the melanoma region (yellow) than the normal region (red).

3.3. Analysis of Refractive Index and Absorption Coefficient

An in-depth analysis of the detected THz time-domain electric field signal was carried out to understand why the melanoma region and normal region of the mouse skin tissue can be differentiated by THz spectroscopy imaging from the perspective of optical physics. To do this, two key physical parameters, i.e., the refractive index and the absorption coefficient, were extracted from the detected THz time-domain electric field signals in which the satellite pulse signals have been filtered out (see below). To help understand the analysis, a schematic was drawn in Fig. 4(a) to show the transmission of THz through the reference and the tissue. The refractive index of the sample, $n_{sam}(f)$, can be calculated via the Eq. (4) [33–35]:

$$n_{sam}(f) = \frac{c\left[\varphi_{sam}(f) - \varphi_{ref}(f)\right]}{2\pi f d} + 1 \tag{4}$$

where c, f, and d, are the speed of the light in the vacuum, frequency of THz wave, and the thickness of the tissue, respectively. $\varphi_{sam}(f)$ and $\varphi_{ref}(f)$ are phase of the sample and the reference obtained from the FFT algorithm of the THz time-domain electric field signal for the sample $E_{sam}(t)$ and the reference $E_{ref}(t)$ via the following two equations:

$$A_{sam}(f)\varphi_{sam}(f) = FFT(E_{sam}(t)) \tag{5}$$

$$A_{ref}(f)\varphi_{ref}(f) = FFT(E_{ref}(t)) \tag{6}$$

where $A_{sam}(f)$ and $A_{ref}(f)$ are the frequency domain amplitude of the sample and the reference, respectively.

The absorption coefficient, $\alpha_{sam}(f)$ of the sample can be obtained by the following equation:

$$\alpha_{sam}(f) = \frac{4\pi f k_{sam}(f)}{c} \tag{7}$$

where $k_{sam}(f)$ is the extinction coefficient deduced from the following equations:

$$k_{sam}(f) = \frac{c}{2\pi f d} \ln\left[T_{sam}(f)\frac{1}{T_{ref}(f)\rho(f)}\right] \tag{8}$$

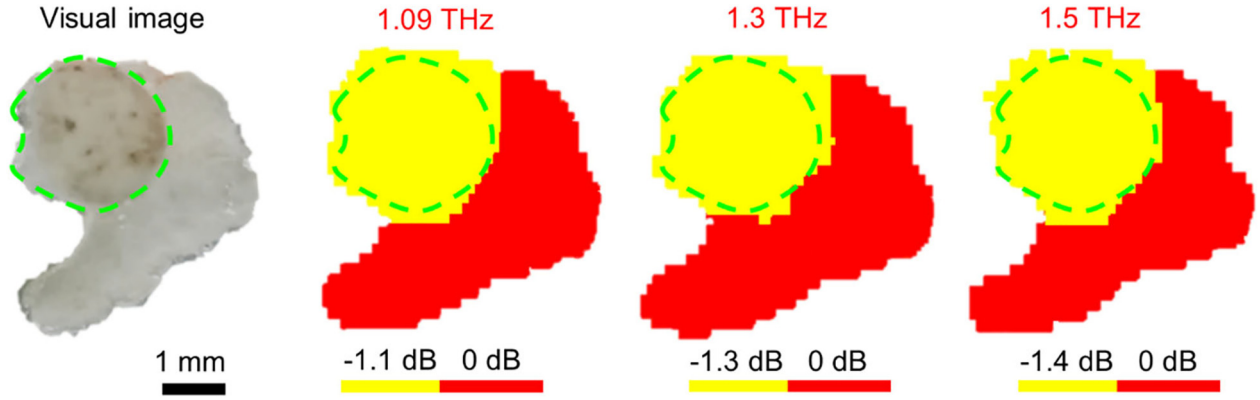

Fig. 3. Optical visual image and corresponding THz images at different frequencies (1.09, 1.3, and 1.5 THz) for a typical mouse skin tissue sample containing melanoma. In the optical visual image, the melanoma region was judged by the darker color and marked out by a green dashed contour line, and other part is the normal region. In THz images, the melanoma region was also indicated by the same green dashed contour line, and the red area corresponds to the normal region. The red color region indicates low THz power-loss while the yellow region indicates high THz power-loss. For the comparison purpose, the power-loss of the normal tissue is set as the reference with a value of '0' dB. (For interpretation of the references to color in this figure legend, the reader is referred to the web version of this article.)

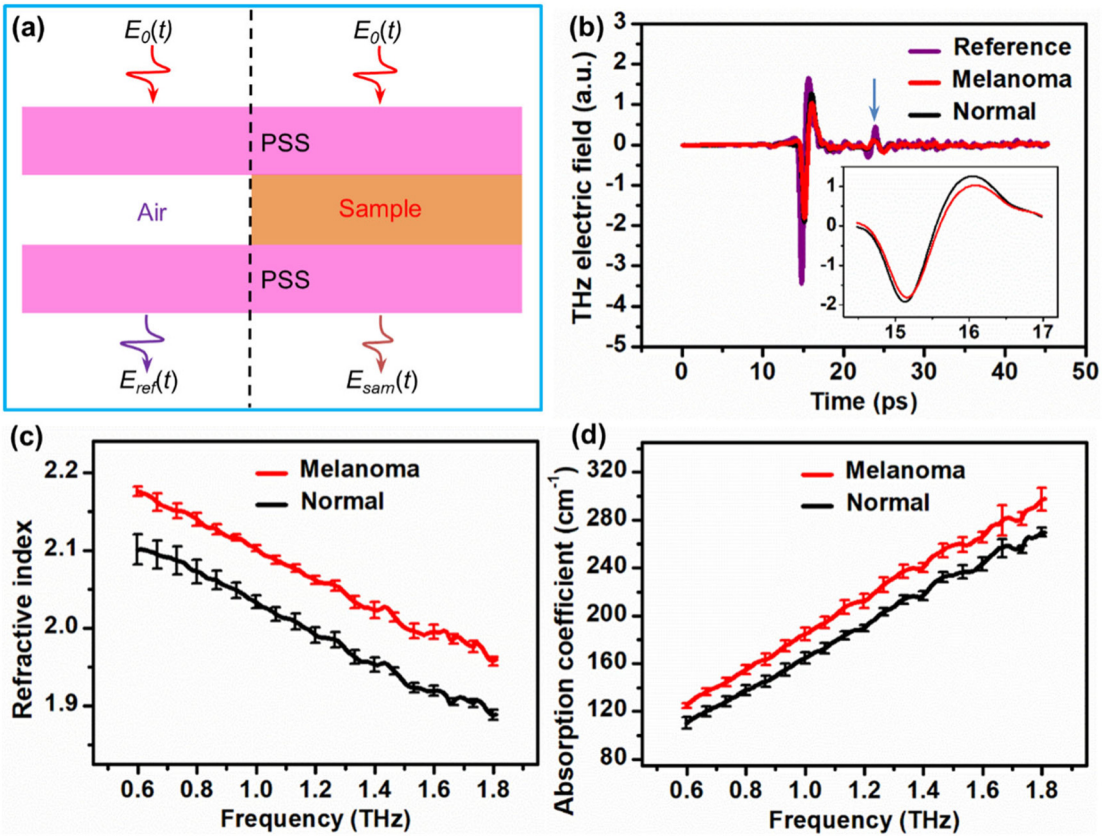

Fig. 4. Refractive index and absorption coefficient obtained from the melanoma region and the normal region of the mouse skin tissue. (a) Schematic showing THz electric fields transmitted through the reference ($E_{ref}(t)$, on the left of the dashed line) and the tissue sample ($E_{sam}(t)$, on the right of the dashed line). The skin tissue was encased in two pieces of polystyrene substrates (PSS). (b) Typical THz time-domain electric field signals with an arbitrary unit for the reference (purple curve), the normal region (black curve) of the tissue and the melanoma region of the tissue (red curve). The satellite pulses (indicated by a blue arrow) have been filtered out by using a Tukey window before the following data analysis. Inset shows the THz electric field signal from 14.5 to 17.0 ps, from which it can be observed that the signal obtained from the normal region is different from the melanoma region. (c) The refractive index and (d) the absorption coefficient for the normal region (black curve) and the melanoma region (red curve) in the frequency range of 0.6–1.8 THz. In the two plots, each point represents the average value of five randomly picked points in the cancerous region or the normal region, and the error bar standards for the standard deviation of the five points. Five different tissue samples obtained from five different BALB/c mice have been measured, and the results are highly consistent. (For interpretation of the references to color in this figure legend, the reader is referred to the web version of this article.)

$$T_{ref}(f) = \frac{4n_{PSS}(f)}{[n_{PSS}(f)+1]^2} \tag{9}$$

$$T_{sam}(f) = \frac{4n_{sam}(f)n_{PSS}(f)}{[n_{sam}(f)+n_{PSS}(f)]^2} \tag{10}$$

$$\rho(f) = \frac{A_{sam}(f)}{A_{ref}(f)} \tag{11}$$

where $n_{PSS}(f)$ is the real part of the refractive index of PSS, $\rho(f)$ is the amplitude ratio of the sample and reference. $T_{ref}(f)$ and $T_{sam}(f)$ are transmissivity of the reference (air-PSS interface) and the sample (tissue-PSS interface). The real part of the refractive index of air was set as '1' in the Eq. (9).

Fig. 4(b) shows typical THz time-domain electric field signals for the reference (purple curve), the normal region of the tissue (black curve) and the melanoma region of the tissue (red curve). It was clearly shown that the THz pulse was changed after the THz wave transmitted through the tissue sample, compared to the reference. The pulses transmission through the tissue sample for both the melanoma region and the normal region were delayed more than reference, indicating higher refractive index of the sample than the reference (air). The peaks of the electric field for the sample were also decreased obviously, compared to the reference, indicating more energy was absorbed by the tissue sample. These results are reasonable because biological tissues normally have a higher refractive index and stronger THz absorption coefficient than air. Before further analysis of the obtained THz time-domain signals, the satellite pulse signals (indicated by a blue arrow) were filtered out by using a Tukey window [36] starting at 0 ps, with a smoothness parameter of 0.1 and a width of 22 ps.

More importantly, it was observed from the inset of Fig. 4(b) that the THz wave transmitted through the melanoma region is different from that transmitted through the normal region. The time delay of THz pulse for melanoma region is relatively larger than that of normal region tissue, indicating larger refractive index of melanoma than that of the normal tissue. It can also be seen that the peak amplitude of THz pulse transmitted through melanoma is lower than that of normal tissue, implying stronger THz absorption of melanoma than the normal tissue.

The refractive index and absorption coefficient for the frequency range of 0.6–1.8 THz were analyzed according to Eqs. (4) and (7) after the removal of the absorption lines of water vapor [37] from the amplitude-frequency spectral data and phase-frequency spectral data at specific frequencies by linear interpolation of their neighboring data, respectively. As shown in Fig. 4(c) and (d), the refractive index and absorption coefficient of melanoma are larger than those of normal tissue, correspondingly. Although the THz electric field can be detected for the frequency between 0.1 and 0.6 THz, the edge artifact in this frequency range is notable due to long wavelength; therefore we did not use the corresponding data in this range to differentiate melanoma and normal tissue. On the other hand, for the frequency larger than 1.8 THz, the power of THz wave transmitted through the sample is

weak, thus the data in this frequency range have not been further analyzed. In fact, the frequency between 0.6 and 1.8 THz is wide enough for the identification of melanoma and normal tissues. It is a common practice to choose a best frequency range to discern different regions in THz-based biological studies. For example, Yamaguchi et al. [22] adopted the frequency range of 0.8 to 1.5 THz to identify brain tumor using the refractive index and absorption coefficient.

3.4. Underlying Mechanisms of Detecting Melanoma Tissue

In pioneering work, it has been suggested that compositional differences between the normal and tumor regions is the origin for contrasted THz signals [38]. Yamaguchi et al. believed that water content and the amount of nucleic acids (cell density) are responsible for the detected THz signals for rat brain tumor and normal regions [23,38]. In addition, proteins and extracellular matrix may also contribute to the difference of THz signals for different tissue regions [17]. However, the current available knowledge in this regard is still very preliminary, and more work is required to interrogate the origin of THz signal difference for tumor and normal tissues, particularly true to for melanoma detection.

By considering the above reasons, we performed HE staining and mass weighing experiments to examine the compositional difference between the melanoma and normal regions of the mouse skin tissue. Mouse skin tissues containing melanoma and normal tissue (adipose/fatty tissue, dermis and epidermis) were evaluated by HE staining. A typical example is shown in Fig. 2(b), from which three major regions can be identified, i.e., the melanoma region (marked by 'M'), adipose region (marked by 'A') and dermis and epidermis layer (marked by 'D'). Compared to the dermis layer, the epidermis layer is very thin and can be neglected. The blue purple dots in the image indicate the location of cell nuclei (Fig. 2(c)), by which it can be seen that the cell density in the melanoma region is much higher than that in the adipose region. More specifically, for an area of 100 μm × 50 μm, the average cell number in the melanoma is 33 ± 5, significant higher than that in the adipose with a number of 16 ± 2. The data are the statistical results of 30 different areas from five different samples. It has been well-established that commonly more cells are existing in the cancerous region than in normal region of a tissue because that cancerous cells are dividing faster than normal cells, resulting in a high cell density in the cancerous region [38,39].

The dermis and epidermis layer is very thin [40] and lies at the most outside of the sample, so it has not been analyzed in our THz spectroscopy imaging due to the spatial resolution of THz technique and the intrinsic edge effect in THz measurements. Therefore, we mainly focus on the analysis of the compositional difference between the adipose and melanoma regions in the following context.

Based on the HE staining results, we can safely say that the nucleus acid/cell density in melanoma is much higher than that in the adipose region. Furthermore, the components of adipose tissue are quite different from melanoma developed from melanoma cells (murine B16) because the adipose tissue consists of a vast range of cellular and noncellular components, such as adipocytes containing large globules of fat, supporting cells comprised of fibroblasts, preadipocytes, cells with mesenchymal and hematopoietic stem cell capacity, structural network of fibers, and so on [41].

From the above discussions, it is evident that the composition in melanoma is very different from the adipose; pronouncedly, the melanoma region has a higher nucleic acids density and water content, and lower fat content than the adipose region. The difference in water content for the melanoma and normal tissue was further confirmed experimentally using a mass weighing method. Since it is technically difficult to assess the water content of the tissue fixed by PFA, we measured the water content of the normal region and the melanoma region of 30 fresh tissue samples excised from 30 mice bearing melanoma, which can give an accurate water content of the normal tissue and melanoma. The fixation of the tissue sample using PFA might influence the water content of the sample; however it is unlikely to influence much on the THz signal, and to change the general trend of the THz image. This could be supported by the work of Sy. et al. [42], in which the authors found that the differences between the fresh and formalin fixed tissue samples were within ~10% for the THz absorption coefficient and within ~3% for refractive index. They also found that diseased and normal regions could still be clearly and correctly identified, no matter the sample was fresh or fixed. According to Eqs. (1)–(3), it was obtained that the water content for melanoma is 82.05 ± 0.2%, significantly higher than that of 62.86 ± 0.5% for the normal tissue (Fig. 5). The water content in melanoma is highly consistent with the water content in rat liver cirrhotic tumor (81–83%) [42]. Since it is difficult to separate the dermis from the adipose of the mouse skin tissue, we measured the water content of the whole normal tissue containing dermis and epidermis. Because the dermis has a water content of ~70% [40] and adipose has a water content of ~30% [43], therefore the measured water content of the normal mouse skin tissue, i.e., 62.86 ± 0.5%, is much higher than pure adipose. In any case, our results do prove that the water content in the melanoma region is higher than the adipose region, due to that the dermis has a much higher water content than the adipose.

Once confirmed the compositional difference between the melanoma region and the adipose region, the refractive index and absorption coefficient extracted from THz transmission signal can be interpreted by the following reasons. First, higher material intensity generally means higher refractive index [22]; therefore higher nucleic acids density found in the melanoma region than the adipose region is consistent with higher refractive index for melanoma. Second, according to Yamauchi et al., higher water content can lead to higher refractive index as well as higher absorption coefficient [22,38,44]. We have quantified that melanoma has much higher water content than the adipose, which is consistent with that melanoma region has a higher refractive index and absorption coefficient than the adipose region. Third, fat (triglyceride) is essentially a nonpolar molecule, which has a smaller absorption coefficient and lower refractive index than polar molecules like water [45]. Since melanoma region has much lower fat content than the adipose region, it is not strange that the melanoma region has a higher absorption coefficient and refractive index than the adipose region. Finally, other compositions such as, melanin [46], proteins, and extracellular matrix may also contribute to the contrasted THz signals for the melanoma region and the normal region; however it is out of the scope of this work and will be investigated in the near future.

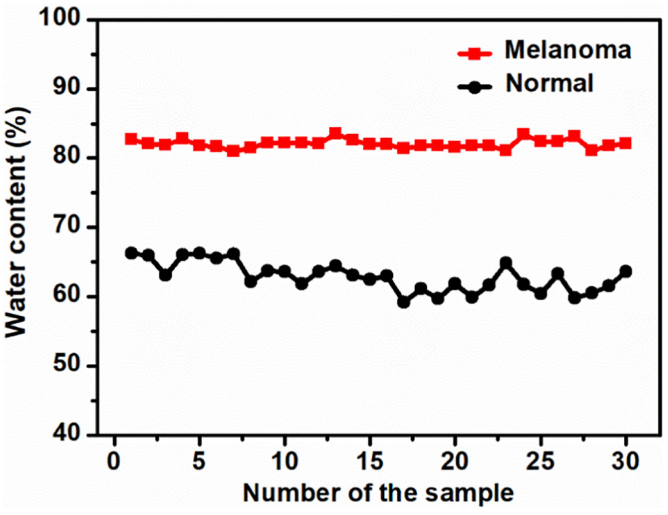

Fig. 5. Plots of water content for the melanoma region and normal region of mouse skin tissues. 30 samples were measured for either melanoma or normal tissue.

4. Conclusions

We have employed the transmission mode THz-TDS system to detect melanoma from the mouse skin tissue. The results show that the melanoma region can be clearly identified using the THz-TDS imaging technique in the range of 0.6–1.8 THz. By an in-depth analysis, it was found that melanoma has higher refractive index and absorption coefficient than the normal skin tissue in this frequency range, which may be very likely due to compositional differences between the tumor and the normal tissue. Namely, melanoma has a higher nucleic acids density, higher water content, and lower fat content than the normal tissue (adipose). This study confirms that it is possible to discriminate melanoma from normal skin tissues, both theoretically and technically. In principle, the technique demonstrated in this work should also be applicable to identity other tumors.

Declaration of Competing Interest

The authors declare that they have no known competing financial interests or personal relationships that could have appeared to influence the work reported in this paper.

Acknowledgements

This work was supported by the National Key Research and Development Program of China (2017YFF0106303), the Central Government Supported Key Instrument Program of China (YXGYQ201700136), the National Natural Science Foundation of China (11604332, 31571782, and 31771975), the Natural Science Foundation of Chongqing (cstc2018jcyjAX0765 and cstc2018jcyjAX0405), the 'Light of West China' Program of Chinese Academy of Sciences (R52A500Z10), and the Chongqing Collaborative Innovation Center for Brain Science.

References

[1] H. Tsao, M.B. Atkins, A.J. Sober, Management of cutaneous melanoma, New Eng. J. Med. 351 (10) (2004) 998–1012, Sep https://doi.org/10.1056/NEJMra041245.
[2] S. Seidenari, C. Ferrari, S. Borsari, E. Benati, G. Ponti, S. Bassoli, F. Giusti, S. Schianchi, G. Pellacani, Reticular grey-blue areas of regression as a dermoscopic marker of melanoma in situ, Brit. J. Dermatol. 163 (2) (2010) 302–309, Aug https://doi.org/10.1111/j.1365-2133.2010.09821.x.
[3] R.L. Siegel, K.D. Miller, A. Jemal, Cancer statistics, 2019, CA Cancer J. Clin. 69 (1) (Jan.-Feb. 2019) 7–34, https://doi.org/10.3322/caac.21551.
[4] H. Ganster, A. Pinz, R. Rohrer, E. Wildling, M. Binder, H. Kittler, Automated melanoma recognition, IEEE Trans. Med. Imaging 20 (3) (2001) 233–239, Mar https://doi.org/10.1109/42.918473.
[5] D.S. Rigel, J. Russak, R. Friedman, The evolution of melanoma diagnosis: 25 years beyond the ABCDs, CA Cancer J. Clin. 60 (5) (Sep.-Oct. 2010) 301–316, https://doi.org/10.3322/caac.20074.
[6] F.M. Walter, A.T. Prevost, J. Vasconcelos, P.N. Hall, N.P. Burrows, H.C. Morris, A.L. Kinmonth, J.D. Emery, Using the 7-point checklist as a diagnostic aid for pigmented skin lesions in general practice: a diagnostic validation study, Brit. J. Gen. Pract. 63 (610) (2013) 345–353, May https://doi.org/10.3399/bjgp13X667213.
[7] C. Herman, Emerging technologies for the detection of melanoma: achieving better outcomes, Clin. Cosmet. Invest. Dermatol. 5 (2012) 195–212, Nov https://doi.org/10.2147/ccid.s27902.
[8] T. Nagatsuma, H. Nishii, T. Ikeo, Terahertz imaging based on optical coherence tomography, Photon. Res. 2 (4) (2014) B64–B69, Aug https://doi.org/10.1364/prj.2.000b64.
[9] A. Schneider, M. Neis, M. Stillhart, B. Ruiz, R.U.A. Khan, P. Gunter, Generation of terahertz pulses through optical rectification in organic DAST crystals: theory and experiment, J. Opt. Soc. Am. B-Opt. Phys. 23 (9) (2006) 1822–1835, Sep https://doi.org/10.1364/josab.23.001822.
[10] W.N. Wang, H.T. Yan, W.W. Yue, G.Z. Zhao, C.L. Zhang, H.B. Liu, X.C. Zhang, THz spectrum of reduced glutathione, Sci. China Ser. G-Phys. Mech. Astron. 48 (5) (2005) 585–592, Oct https://doi.org/10.1360/142005-32.
[11] Z.B. Yang, S.L. Feng, W. Yao, J.G. Han, H.B. Wang, Synthesis of novel rambutan-like graphene@aluminum composite spheres and non-destructive terahertz characterization, RSC Adv. 9 (6) (2019) 3486–3492, Jan https://doi.org/10.1039/c8ra09129c.
[12] X. Yang, X. Zhao, K. Yang, Y.P. Liu, Y. Liu, W.L. Fu, Y. Luo, Biomedical applications of terahertz spectroscopy and imaging, Trends Biotechnol. 34 (10) (2016) 810–824, Oct https://doi.org/10.1016/j.tibtech.2016.04.008.
[13] R. Zhang, L.L. Zhang, T. Wu, R.X. Wang, S.S. Zuo, D. Wu, C.L. Zhang, J. Zhang, J. Fang, Continuous-terahertz-wave molecular imaging system for biomedical applications, J. Biomed. Opt. 21 (7) (Jul. 2016), 076006. https://doi.org/10.1117/1.jbo.21.7.076006.
[14] O.A. Smolyanskaya, N.V. Chernomyrdin, A.A. Konovko, K.I. Zaytsev, I.A. Ozheredov, O.P. Cherkasova, M.M. Nazarov, J.P. Guillet, S.A. Kozlov, Y.V. Kistenev, J.L. Coutaz, P. Mounaix, V.L. Vaks, J.H. Son, H. Cheon, V.P. Wallace, Y. Feldman, I. Popov, A.N. Yaroslavsky, A.P. Shkurinov, V.V. Tuchin, Terahertz biophotonics as a tool for studies of dielectric and spectral properties of biological tissues and liquids, Prog. Quant. Electron. 62 (2018) 1–77, Nov https://doi.org/10.1016/j.pquantelec.2018.10.001.
[15] K.I. Zaytsev, I.N. Dolganova, N.V. Chernomyrdin, G.M. Katyba, A.A. Gavdush, O.P. Cherkasova, G.A. Komandin, M.A. Shchedrina, A.N. Khodan, D.S. Ponomarev, I.V. Reshetov, V.E. Karasik, M. Skorobogatiy, V.N. Kurlov, V.V. Tuchin, The progress and perspectives of terahertz technology for diagnosis of neoplasms: a review, J. Opt. 22 (1) (2019) 1–50, Dec https://doi.org/10.1088/2040-8986/ab4dc3.
[16] S.J. Oh, S.H. Kim, K. Jeong, Y. Park, Y.M. Huh, J.H. Son, J.S. Suh, Measurement depth enhancement in terahertz imaging of biological tissues, Opt. Express 21 (18) (2013) 21299–21305, Sep https://doi.org/10.1364/oe.21.021299.
[17] H.L. Zhao, Y.Y. Wang, L.Y. Chen, J. Shi, K. Ma, L.H. Tang, D.G. Xu, J.Q. Yao, H. Feng, T.N. Chen, High-sensitivity terahertz imaging of traumatic brain injury in a rat model, J. Biomed. Opt. 23 (3) (2018) 1–7, Mar https://doi.org/10.1117/1.jbo.23.3.036015.
[18] J. Shi, Y.Y. Wang, T.N. Chen, D.G. Xu, H.L. Zhao, L.Y. Chen, C. Yan, L.H. Tang, Y.X. He, H. Feng, J.Q. Yao, Automatic evaluation of traumatic brain injury based on terahertz imaging with machine learning, Opt. Express 26 (5) (2018) 6371–6381, Mar https://doi.org/10.1364/oe.26.006371.
[19] A.J. Fitzgerald, S. Pinder, A.D. Purushotham, P. O'Kelly, P.C. Ashworth, V.P. Wallace, Classification of terahertz-pulsed imaging data from excised breast tissue, J. Biomed. Opt. 17 (1) (Jan. 2012), 016005. https://doi.org/10.1117/1.jbo.17.1.016005.
[20] M.A. Brun, F. Formanek, A. Yasuda, M. Sekine, N. Ando, Y. Eishii, Terahertz imaging applied to cancer diagnosis, Phys. Med. Biol. 55 (16) (2010) 4615–4623, Aug https://doi.org/10.1088/0031-9155/55/16/001.
[21] A.A. Gavdush, N.V. Chernomyrdin, K.M. Malakhov, S.T. Beshplav, I.N. Dolganova, A.V. Kosyrkova, P.V. Nikitin, G.R. Musina, G.M. Katyba, I.V. Reshetov, O.P. Cherkasova, G.A. Komandin, V.E. Karasik, A.A. Potapov, V.V. Tuchin, K.I. Zaytsev, Terahertz spectroscopy of gelatin-embedded human brain gliomas of different grades: a road toward intraoperative THz diagnosis, J. Biomed. Opt. 24 (2) (Feb. 2019), 027001. https://doi.org/10.1117/1.JBO.24.2.027001.
[22] S. Yamaguchi, Y. Fukushi, O. Kubota, T. Itsuji, T. Ouchi, S. Yamamoto, Brain tumor imaging of rat fresh tissue using terahertz spectroscopy, Sci. Rep. 6 (Jul. 2016), 30124. https://doi.org/10.1038/srep30124.
[23] S.J. Oh, S.H. Kim, Y.B. Ji, K. Jeong, Y. Park, J. Yang, D.W. Park, S.K. Noh, S.G. Kang, Y.M. Huh, J.H. Son, J.S. Suh, Study of freshly excised brain tissues using terahertz imaging, Biomed. Opt. Express 5 (8) (2014) 2837–2842, Aug https://doi.org/10.1364/boe.5.002837.
[24] K.I. Zaytsev, K.G. Kudrin, V.E. Karasik, I.V. Reshetov, S.O. Yurchenko, In vivo terahertz spectroscopy of pigmentary skin nevi: pilot study of non-invasive early diagnosis of dysplasia, Appl. Phys. Lett. 106 (5) (Feb. 2015), 053702. https://doi.org/10.1063/1.4907350.
[25] J.Y. Park, H.J. Choi, H. Cheon, S.W. Cho, S. Lee, J.H. Son, Terahertz imaging of metastatic lymph nodes using spectroscopic integration technique, Biomed. Opt. Express 8 (2) (2017) 1122–1129, Feb https://doi.org/10.1364/boe.8.001122.
[26] K.G. Dernby, A study on autolysis of animal tissues, J. Biol. Chem. 35 (2) (1918) 179–219, Aug.
[27] T.C. Bowman, M. El-Shenawee, L.K. Campbell, Terahertz imaging of excised breast tumor tissue on paraffin sections, IEEE Trans. Antenn. Propag. 63 (5) (2015) 2088–2097, May https://doi.org/10.1109/tap.2015.2406893.
[28] G.S. Geng, G.B. Dai, D.D. Li, S.L. Zhou, Z.X. Li, Z.B. Yang, Y.H. Xu, J.G. Han, T.Y. Chang, H.-L. Cui, H.B. Wang, Imaging brain tissue slices with terahertz near-field microscopy, Biotechnol. Prog. 35 (2) (Dec. 2019), e2741. https://doi.org/10.1002/btpr.2741.
[29] C.S. Joseph, R. Patel, V.A. Neel, R.H. Giles, A.N. Yaroslavsky, Imaging of ex vivo nonmelanoma skin cancers in the optical and terahertz spectral regions, J. Biophotonics 7 (5) (May 2014) 295–303, https://doi.org/10.1002/jbio.201200111.
[30] K.R. Bambery, E. Schultke, B.R. Wood, S.T.R. MacDonald, K. Ataelmannan, R.W. Griebel, B.H.J. Juurlink, D. McNaughton, A Fourier transform infrared micro spectroscopic imaging investigation into an animal model exhibiting glioblastoma multiforme, BBA-Biomembranes 1758 (7) (2006) 900–907, Jul https://doi.org/10.1016/j.bbamem.2006.05.004.
[31] Y.X. Wang, Z.R. Zhao, Z.Q. Chen, L. Zhang, K.J. Kang, J.K. Deng, Z.F. Huang, Diffraction enhanced imaging with pulsed terahertz radiation, Proc. IEEE Nucl. Sci. Sym. Conf. Rec., Orlando, FL, USA, 1–5, 2009, pp. 2465–2468 , no. 1-5. Oct https://doi.org/10.1109/NSSMIC.2009.5402100.
[32] R. Biswas, W. Bae, E. Diaz, K. Masuda, C.B. Chung, G.M. Bydder, J. Du, Ultrashort echo time (UTE) imaging with bi-component analysis: bound and free water evaluation of bovine cortical bone subject to sequential drying, Bone 50 (3) (2012) 749–755, Mar https://doi.org/10.1016/j.bone.2011.11.029.
[33] X. Yang, D.S. Wei, S.H. Yan, Y.P. Liu, S. Yu, M.K. Zhang, Z.B. Yang, X.Y. Zhu, Q. Huang, H.-L. Cui, W.L. Fu, Rapid and label-free detection and assessment of bacteria by terahertz time-domain spectroscopy, J. Biophotonics 9 (10) (2016) 1050–1058, Oct https://doi.org/10.1002/jbio.201500270.
[34] S.H. Yan, D.S. Wei, M.J. Tang, C.C. Shi, M.K. Zhang, Z.B. Yang, C.L. Du, H.-L. Cui, Determination of critical micelle concentrations of surfactants by terahertz time-domain spectroscopy, IEEE Trans. THz Sci. Technol. 6 (4) (2016) 532–540, Jul https://doi.org/10.1109/tthz.2016.2575450.
[35] P.C. Ashworth, E. Pickwell-MacPherson, E. Provenzano, S.E. Pinder, A.D. Purushotham, M. Pepper, V.P. Wallace, Terahertz pulsed spectroscopy of freshly excised human breast cancer, Opt. Express 17 (15) (2009) 12444–12454, Jul https://doi.org/10.1364/oe.17.012444.

[36] B.M. Giuliano, A.A. Gavdush, B. Muller, K.I. Zaytsev, T. Grassi, A.V. Ivlev, M.E. Palumbo, G.A. Baratta, C. Scire, G.A. Komandin, S.O. Yurchenko, P. Caselli, Broadband spectroscopy of astrophysical ice analogues I. direct measurement of the complex refractive index of CO ice using terahertz time-domain spectroscopy, Astron. Astrophys. 629 (Sep. 2019), A112. https://doi.org/10.1051/0004-6361/201935619.

[37] A. Roggenbuck, H. Schmitz, A. Deninger, I.C. Mayorga, J. Hemberger, R. Gusten, M. Gruninger, Coherent broadband continuous-wave terahertz spectroscopy on solid-state samples, New J. Phys. 12 (Apr. 2010), 043017. https://doi.org/10.1088/1367-2630/12/4/043017.

[38] S. Yamaguchi, Y. Fukushi, O. Kubota, T. Itsuji, T. Ouchi, S. Yamamoto, Origin and quantification of differences between normal and tumor tissues observed by terahertz spectroscopy, Phys. Med. Biol. 61 (18) (2016) 6808–6820, Sep https://doi.org/10.1088/0031-9155/61/18/6808.

[39] F. Wahaia, I. Kasalynas, D. Seliuta, G. Molis, A. Urbanowicz, C.D.C. Silva, F. Carneiro, G. Valusis, P.L. Granja, Terahertz spectroscopy for the study of paraffin-embedded gastric cancer samples, J. Mol. Struct. 1079 (2015) 391–395, Jan https://doi.org/10.1016/j.molstruc.2014.09.002.

[40] M. Guzman-Alonso, T.M. Cortazar, Water content at different skin depths and the influence of moisturizing formulations, Household Pers. Care Today 11 (Jan.-Feb. 2016) 35–40.

[41] G. Martinez-Santibanez, K.W. Cho, C.N. Lumeng, Imaging ehite adipose tissue with confocal microscopy, in: O.A. MacDougald (Ed.), Methods of Adipose Tissue Biology, Methods in Enzymology, Pt A, 537, Elsevier Academic Press Inc, San Diego 2014, pp. 17–30.

[42] S. Sy, S. Huang, Y.X.J. Wang, J. Yu, A.T. Ahuja, Y.T. Zhang, E. Pickwell-MacPherson, Terahertz spectroscopy of liver cirrhosis: investigating the origin of contrast, Phys. Med. Biol. 55 (24) (2010) 7587–7596, Dec https://doi.org/10.1088/0031-9155/55/24/013.

[43] Y.Z. He, B.S.Y. Ung, E.P.J. Parrott, A.T. Ahuja, E. Pickwell-MacPherson, Freeze-thaw hysteresis effects in tetrahertz imaging of biomedical tissues, Biomed. Opt. Express 7 (11) (2016) 4711–4717, Nov https://doi.org/10.1364/boe.7.004711.

[44] R. Zhang, K. Yang, B. Yang, N.A. AbuAli, M. Hayajneh, M. Philpott, Q.H. Abbasi, A. Alomainy, Dielectric and double debye parameters of artificial normal skin and melanoma, J. Infrared Millim. THz Wave 40 (6) (2019) 657–672, Jun https://doi.org/10.1007/s10762-019-00597-x.

[45] T. Bowman, M. El-Shenawee, L.K. Campbell, Terahertz transmission vs reflection imaging and model-based characterization for excised breast carcinomas, Biomed. Opt. Express 7 (9) (2016) 3756–3783, Sep https://doi.org/10.1364/boe.7.003756.

[46] X.G. Peralta, D. Lipscomb, G.J. Wilmink, I. Echchgadda, Terahertz spectroscopy of human skin tissue models with different melanin content, Biomed. Opt. Express 10 (6) (2019) 2942–2955, Jun https://doi.org/10.1364/BOE.10.002942.